AGU PUBLICATIONS

Space Weather

RESEARCH ARTICLE
10.1002/2017SW001779

Key Points:
- The use of empirical 3-D impedances produces significant spatial variability in the voltages that are calculated across transmission lines
- Calculation of voltages across transmission lines during the March 1989 storm shows numerous transmission lines exceeding 100 V
- Integrating over transmission lines does not always reduce the influence of spatial geoelectric variability caused by realistic impedances

Supporting Information:
- Supporting Information S1
- Movie S1
- Movie S2

Correspondence to:
G. Lucas,
glucas@usgs.gov

Citation:
Lucas, G. M., Love, J. J., & Kelbert, A. (2018). Calculation of voltages in electric power transmission lines during historic geomagnetic storms: An investigation using realistic earth impedances. *Space Weather*, *16*, 185–195. https://doi.org/10.1002/2017SW001779

Received 20 NOV 2017
Accepted 14 JAN 2018
Accepted article online 14 FEB 2018
Published online 26 FEB 2018

Calculation of Voltages in Electric Power Transmission Lines During Historic Geomagnetic Storms: An Investigation Using Realistic Earth Impedances

Greg M. Lucas[1], **Jeffrey J. Love**[1], **and Anna Kelbert**[1]

[1] Geomagnetism Program, U.S. Geological Survey, Denver, CO, USA

Abstract Commonly, one-dimensional (1-D) Earth impedances have been used to calculate the voltages induced across electric power transmission lines during geomagnetic storms under the assumption that much of the three-dimensional structure of the Earth gets smoothed when integrating along power transmission lines. We calculate the voltage across power transmission lines in the mid-Atlantic region with both regional 1-D impedances and 64 empirical 3-D impedances obtained from a magnetotelluric survey. The use of 3-D impedances produces substantially more spatial variance in the calculated voltages, with the voltages being more than an order of magnitude different, both higher and lower, than the voltages calculated utilizing regional 1-D impedances. During the March 1989 geomagnetic storm 62 transmission lines exceed 100 V when utilizing empirical 3-D impedances, whereas 16 transmission lines exceed 100 V when utilizing regional 1-D impedances. This demonstrates the importance of using realistic impedances to understand and quantify the impact that a geomagnetic storm has on power grids.

1. Introduction

Geomagnetic storms induce geoelectric fields within the electrically conducting interior of the Earth that produce voltages across grounded transmission lines. These voltages can lead to severe impacts on the transmission of electricity (Boteler, 2001; Molinski, 2002; Piccinelli & Krausmann, 2014; Samuelsson, 2013). A geomagnetic storm on 13 March 1989 caused a widespread blackout in Canada with the collapse of the Hydro-Québec power system (Bolduc, 2002) and caused numerous anomalies and faults within the United States (U.S.) power transmission network (North American Electric Reliability Corporation, 1990). With modern society's increasing reliance on electricity, some studies estimate that a large geomagnetic storm could have severe economic impacts (National Research Council, 2008). In light of the risks associated with geomagnetic storms, the *Federal Energy Regulatory Commission* of the United States has directed an investigation into the vulnerability of the U.S. power grid to geomagnetic disturbances (Federal Energy Regulatory Commission, 2013).

Several complex processes are involved in determining the impact of geomagnetic storms on the electric power grid. These processes include the induction of geoelectric fields in the solid Earth by geomagnetic variations, the calculation of voltages (potential differences) across power transmission lines, and the generation of currents within the power grid itself (e.g., Electric Power Research Institute, 2013; North American Electric Reliability Corporation, 2013a; Price, 2002). Modeling current flow within a power grid network requires a detailed knowledge of the interconnections and resistances of the power transmission lines (e.g., North American Electric Reliability Corporation, 2013b; Overbye et al., 2013; Shetye & Overbye, 2015), which is often proprietary information. There are several detailed software simulation packages for calculating the distribution of currents within the power grid that are already developed and used within the industry. All of these software packages take the geoelectric field or voltages across transmission lines as an input and then calculate the resultant currents with the detailed knowledge of the power grid geometry and properties (e.g., Boteler, 2014; Marti et al., 2013, 2014).

The *North American Electric Reliability Corporation* has developed 100 year benchmark geoelectric fields across the United States (North American Electric Reliability Corporation, 2016) to meet the federal directive addressing the vulnerability of the U.S. power grid to geomagnetic disturbances. These benchmarks are produced by considering large physiographic regions across the United States (e.g., Fernberg, 2012). Assuming no lateral

variability in electrical conductivity within these large regions leads to purely depth-dependent conductivity profiles that produce so-called one-dimensional (1-D) impedances. These profiles are convenient because they encompass large portions of the United States. However, due to their large regions, much of the finer-scale geologic structure is missed. Utilizing empirical 3-D impedance tensors (3-D allows for horizontal variations in conductivity), Love et al. (2016) have shown that there are significant differences in calculated geoelectric fields, even within the same physiographic region.

Several previous analyses have investigated 3-D versus 1-D impedances analyzing the local geoelectric fields produced with synthetic magnetic fields (e.g., Bedrosian & Love, 2015) and real magnetic field time series (e.g., Kelbert et al., 2017; Love et al., 2017; Weigel, 2017). These studies have clearly identified that there are significant differences in the calculated geoelectric fields between 3-D and 1-D impedances. However, a number of issues remain to be explored, such as, whether significant local differences get spatially smoothed when an integration along a power transmission line is performed to calculate the voltage across the transmission line. Long electric power transmission lines can pass over significant variations in Earth's electrical conductivity structure, which requires the use of multiple different impedance tensors to model the spatial variations in geoelectric fields near the surface of the Earth. Analysis of the power grid in Europe has justified the use of 1-D models and the calculation of average geoelectric fields based on the argument that an integration over a transmission line acts as a smoothing operator (e.g., Viljanen et al., 2012). To calculate the voltages across transmission lines, we utilize the mid-Atlantic region which contains many power transmission lines, is well surveyed magnetotellurically, and has a magnetic observatory located within the region.

2. Calculating Voltages

There are multiple steps to calculate the voltages across transmission lines from a geomagnetic field input. The first step is to calculate geoelectric fields at the surface of the Earth. The relationship between the magnetic field and electric field near the surface of the earth can be described through an impedance tensor, **Z**. The impedance tensor has real and imaginary parts, and, assuming a plane wave source magnetic field, has four components to relate the horizontal magnetic field to the horizontal induced geoelectric field.

The calculation of geoelectric fields has commonly been done with regional 1-D impedance tensors (e.g., Boteler & Pirjola, 2017; Electric Power Research Institute, 2013; Marti et al., 2014; North American Electric Reliability Corporation, 2013b; Viljanen et al., 2012). A 1-D impedance is derived from a conductivity profile that is only a function of depth. One-dimensional conductivity profiles are typically derived from a literature survey of regional geology and disparate physical sampling, such as those produced by Fernberg (2012) that cover the United States. The conductivity and depth from the regional models are then utilized within a simple forward model (e.g., Electric Power Research Institute, 2013; Simpson & Bahr, 2005) to calculate the impedance as a function of frequency. The 1-D impedance is skew symmetric with the off-diagonal component, Z, calculated through the forward model, while the 3-D impedance tensor is fully populated.

$$\mathbf{Z}_{1D} = \begin{bmatrix} 0 & Z \\ -Z & 0 \end{bmatrix} \quad \mathbf{Z}_{3D} = \begin{bmatrix} Z_{xx} & Z_{xy} \\ Z_{yx} & Z_{yy} \end{bmatrix}$$

The geoelectric field, ***E***, is calculated through a convolution of the magnetic field, **B**, with the impedance of the Earth in the time domain $\mathbf{E}(t) = \mathbf{Z} * \mathbf{B}(t)$. A Fourier transform of the magnetic field, $\mathbf{B}(\omega) = \mathcal{F}\{\mathbf{B}(t)\}$, is performed to transform this equation into a linear multiplication in the frequency domain

$$\mathbf{E}(\omega) = \mathbf{Z}(\omega)\mathbf{B}(\omega)/\mu, \tag{1}$$

where μ is the local magnetic permeability, typically approximated to the free space value, μ_0.

The calculation of the geolectric field in equation (1) is computed in the frequency domain. To obtain the time variation of the geoelectric field, $\mathbf{E}(t)$, an inverse Fourier transform, $\mathcal{F}^{-1}\{\}$, of the frequency domain geoelectric field is performed,

$$\mathbf{E}(t) = \mathcal{F}^{-1}\{\mathbf{E}(\omega)\} = \mathcal{F}^{-1}\{\mathbf{Z}(\omega)\mathbf{B}(\omega)/\mu\}. \tag{2}$$

The final step in obtaining voltages across transmission lines is to calculate the line integral of the electric field over the geometry of the electric transmission lines

$$V(t) = \int_{\mathrm{L}} \mathbf{E}(t) \cdot \mathrm{d}\mathbf{l}, \tag{3}$$

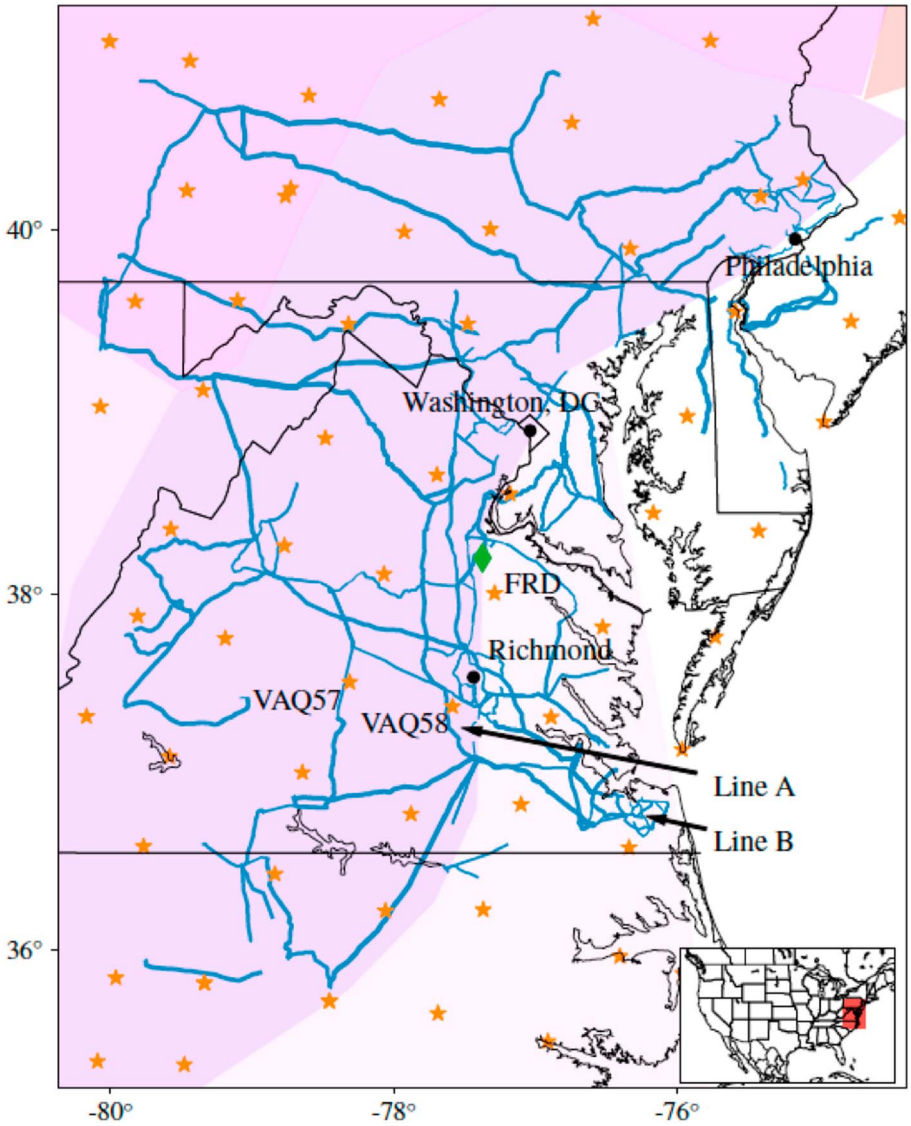

Figure 1. A map of the mid-Atlantic region with several major cities highlighted. The location of this region within the greater United States is highlighted with a red square in the inset figure in the lower right. The transmission lines are in blue, the Fredericksburg geomagnetic observatory is a green diamond in the center of the map, the shaded background corresponds to different 1-D conductivity regions, and the magnetotelluric impedance tensor sites are represented with orange stars, with two specific survey sites listed (VAQ57 and VAQ58).

where d**l** is a path segment along the transmission line, *L*. This voltage represents the potential difference that is generated along a single transmission line between two power substations, which can be utilized by power companies to determine how geomagnetically induced currents flow within their power grid.

3. Data Sources Within the Mid-Atlantic

There are three distinct data sets that are used when computing voltages within an electric power grid. These are the magnetic field at the surface of the Earth, the impedance of the solid Earth, and the geometry and configuration of the transmission lines across the surface of the Earth. Figure 1 shows the region of interest which is centered on a U.S. Geological Survey geomagnetic observatory (Love & Finn, 2011) located in Fredericksburg, Virginia (geographic latitude: 38.205°, geographic longitude: −77.373°, indicated with a green diamond) (geomagnetic latitude: 47.76°, geomagnetic longitude: −5.56°) and encompasses a square region of 3° in latitude and longitude, approximately 600 km by 600 km. An inset figure highlights the mid-Atlantic region in this study with respect to the continental United States. The spatial scales were

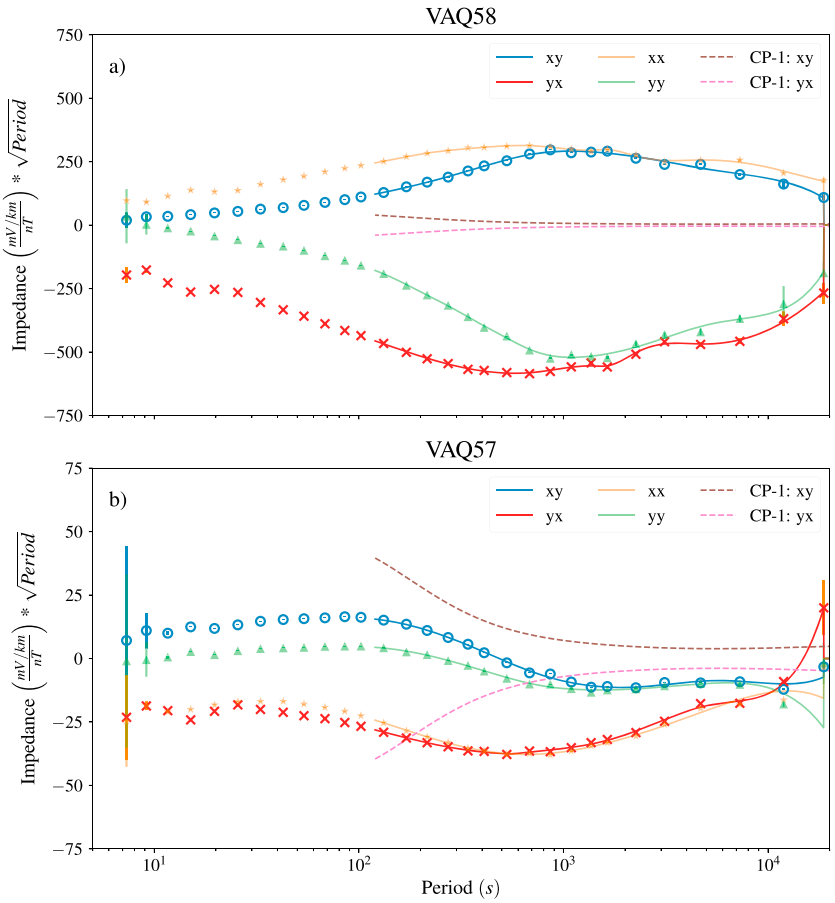

Figure 2. Components of the impedance tensor for two EarthScope sites (a) VAQ58 and (b) VAQ57 and the 1-D model CP-1 (Fernberg, 2012) as a function of the period of the signal. The empirical data are at the discrete points, along with the associated error bars, while the interpolation spline is shown as a solid line. The interpolation begins at 120 s, even though data exist at higher frequencies because of the Nyquist period for the 1 min magnetic field data from FRD. The *y* axes are an order of magnitude different between the two plots despite the close geographic proximity of the two sites indicating the variability of the empirical impedance tensors.

chosen to allow for the assumption of a uniform geomagnetic field throughout the region without needing to use interpolation methods between multiple geomagnetic observatories (e.g., Watermann et al., 2006). This simplification enables the paper to focus on geoelectric fields and voltages rather than complicating the analysis with spatially varying magnetic fields. The Fredericksburg magnetic field data, utilized here, are definitive (they are calibrated and have been processed to remove spikes and offsets) 1 min averages reported at discrete intervals (USGS, 1901). With a plane wave assumption on the magnetic field source, only the horizontal (*x* and *y*) magnetic field components are utilized.

The National Science Foundation EarthScope program has undertaken a magnetotelluric survey across large portions of the United States (Schultz et al., 2006) with a roughly 70 km spacing between each survey site. For each location in the survey, a fluxgate magnetometer and a pair of electrodes in the north/south and east/west directions are deployed to obtain time-coincident measurements of the geomagnetic and geoelectric fields. Measurements at each survey site are typically conducted over a few weeks to obtain enough data for long-period estimates. The measurement of the time-coincident geomagnetic field and geoelectric field provides a method to calculate the impedance tensor as a function of frequency, $\mathbf{Z}(\omega)$ (e.g., Egbert, 2007). Impedance tensors derived from the survey sites cover the range of periods from roughly 10 s to 20,000 s with an estimated error that is generally much smaller than 5% except at the longest periods (Schultz, 2010). The 64 specific EarthScope survey sites used within this analysis are shown with orange stars in Figure 1.

There are numerous high-voltage transmission lines in the mid-Atlantic region shown as blue lines in Figure 1. These transmission lines serve the cities of Philadelphia, Baltimore, Washington D.C., Richmond, and other

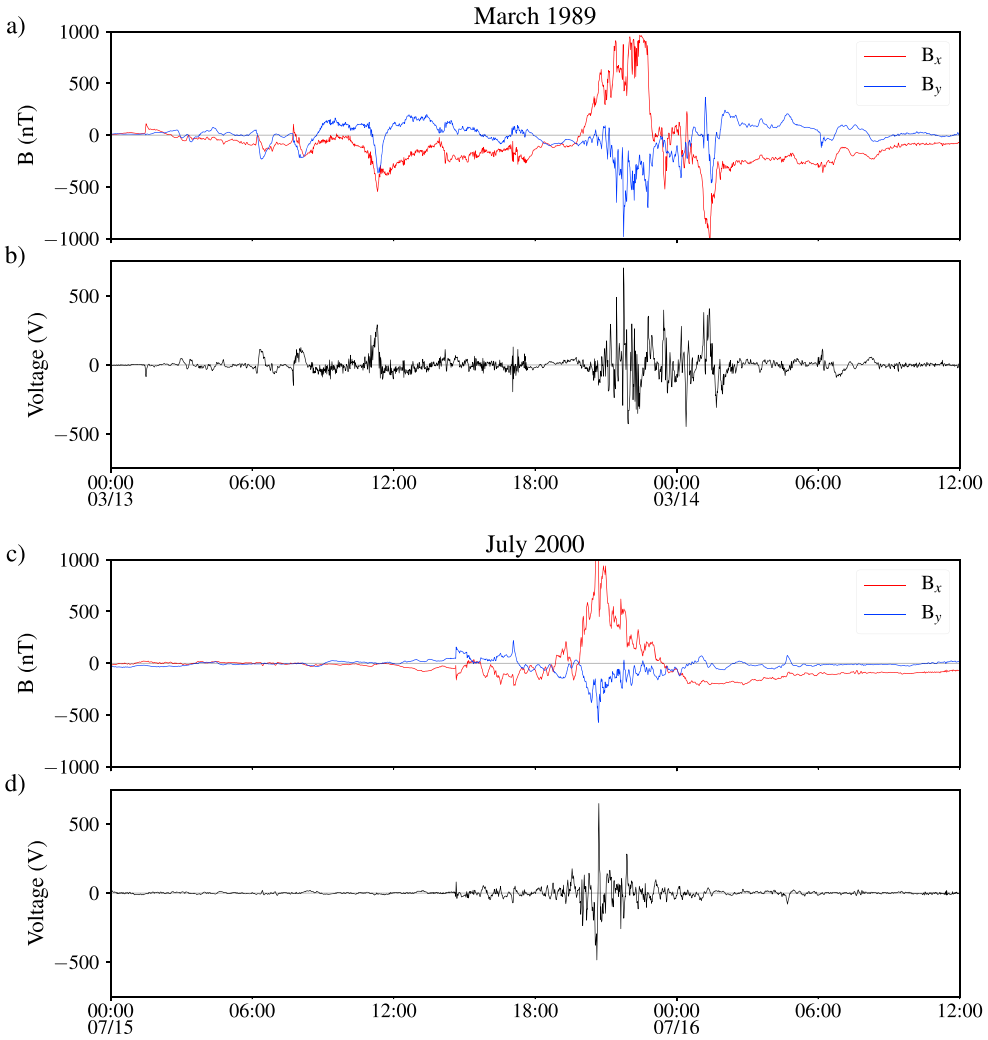

Figure 3. Time series of magnetic fields and voltages across Line A from Figure 1 for two different geomagnetic storms. (a) Magnetic field and (b) voltage during the March 1989 geomagnetic storm. (c) Magnetic field and (d) voltage during the July 2000 geomagnetic storm. The March 1989 geomagnetic storm was both strong and long-lived, and the voltages seen across the power line are large and last for several hours. The July 2000 geomagnetic storm is strong and impulsive, where the large voltages last less than an hour.

large metropolises in the region. Transmission lines can span several orders of magnitude in length between grounding points, from relatively short distances of a few kilometers up to multiple hundreds of kilometers. In this manuscript, only transmission lines that carry voltages over 150 kV within the mid-Atlantic region are considered. The data for the transmission lines are obtained from the Department of Homeland Security and contain the latitude and longitude for many points along each transmission line.

4. Utilizing Data to Calculate Voltages

The geomagnetic field data, $\mathbf{B}(t)$, are detrended with a second-order polynomial least squares fit in each vector component to remove long-period trends from the data. The 3-D impedance tensors, and associated variances, obtained from the EarthScope survey, $\mathbf{Z}$, are parameterized in terms of a discrete set of frequencies. To perform the multiplication in equation (2) the variables $\mathbf{Z}(\omega)$ and $\mathbf{B}(\omega)$ need to be defined over the same set of frequencies. This requires the EarthScope impedances to be estimated at a finer set of frequencies than the data are parameterized with. A least squares spline fit to the impedance tensor data, utilizing the variance from the measurements, in log-frequency space is used to sample the data at a finer-frequency

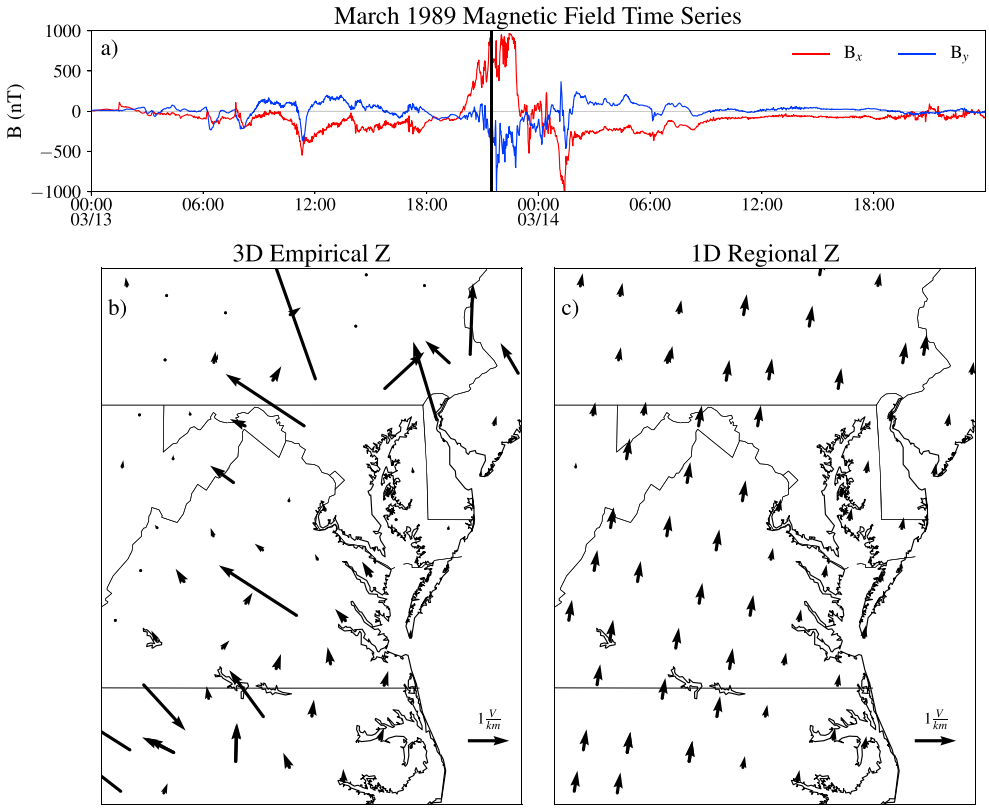

Figure 4. (a) Geomagnetic field at the USGS Fredericksburg geomagnetic observatory during the 1989 geomagnetic storm. (b) Snapshot at 21:30 13 March 1989 of the geoelectric fields at the 64 EarthScope sites that are used to calculate the voltages across transmission lines. (c) The geoelectric fields calculated at those same sites, but using the regional 1-D impedances (Fernberg, 2012). There is variability in both the magnitude and direction of the electric field vectors throughout the region when using empirical 3-D impedances that is not realized through the use of regional 1-D impedances.

resolution. Representative fits are shown through two EarthScope sites (VAQ57 and VAQ58) in Figure 2. The two EarthScope sites are in relatively close spatial proximity, as seen in Figure 1, yet have orders of magnitude difference in their impedances as described in Love et al. (2017).

The electric field calculation in equation (2) is performed at the 64 EarthScope sites in the mid-Atlantic region to obtain 64 time series of electric fields over the region. These are data-derived geoelectric fields over the entire region that are physically representative of the area. Previous studies have investigated the geoelectric fields at the EarthScope sites to develop geoelectric hazard maps (e.g., Love et al., 2016). The geoelectric fields calculated in the hazard maps are for a simulated magnetic field to determine the response at specific frequencies. Recently, these geoelectric hazard maps have been revisited over the mid-Atlantic region utilizing measured geomagnetic fields (Love et al., 2017). Here we are using the time series of calculated geoelectric fields from the observed magnetic field time series for a few historic geomagnetic storms.

The geoelectric field at every point along the transmission line is calculated with two different methods using the calculated geoelectric fields at the 64 EarthScope sites. The first method is using the nearest EarthScope site in a nearest neighbor (NN) fashion, and the second method utilizes a Delaunay triangulation to calculate barycentric interpolation weights between three sites that form a triangle around the point (e.g., Preparata & Shamos, 1993), similar to the method described in Bonner and Schultz (2017). The interpolation for both methods is computed over each vector component, in the north/south and east/west directions, independently. Throughout this paper, the *x* coordinate is defined as positive north and the *y* coordinate as positive east. Equation (3) is used to calculate the voltage across each transmission line from the calculated geoelectric fields along the transmission line.

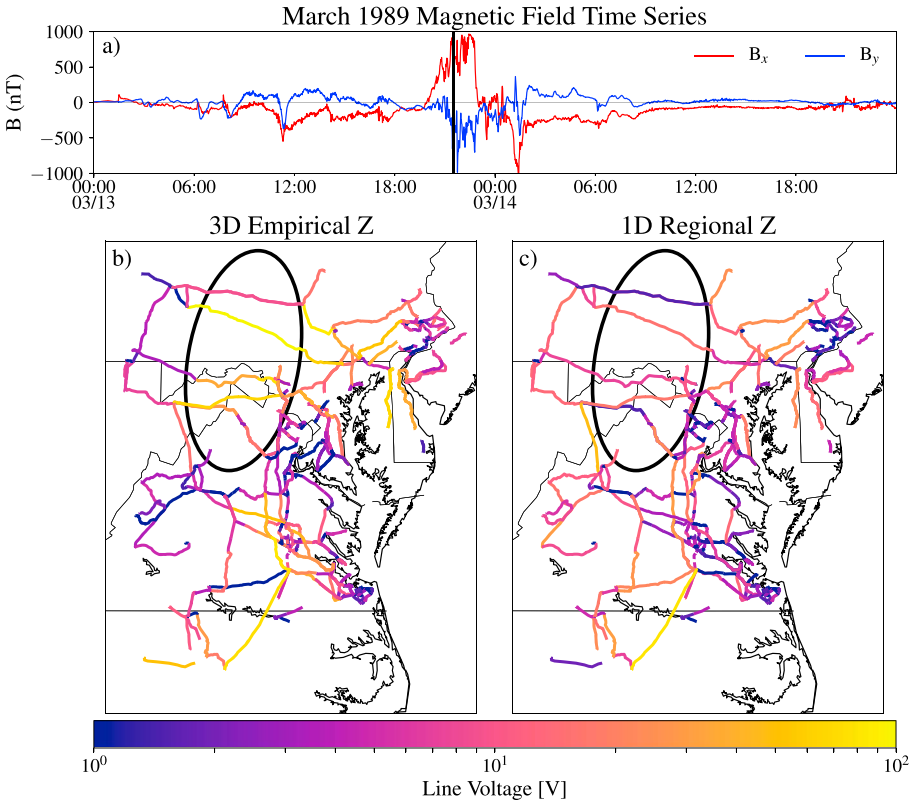

Figure 5. (a) Geomagnetic field at the USGS Fredericksburg geomagnetic observatory during the 1989 geomagnetic storm. (b) Snapshot at 21:30 13 March 1989 of the calculated voltages across the transmission lines in the mid-Atlantic region with the use of empirical 3-D impedances. (c) Calculated voltages across the transmission lines using regional 1-D impedances (Fernberg, 2012). Note that the colormap is logarithmically scaled, indicating the wide range of voltages that are generated across transmission lines. The circled region is an area where the use of empirical 3-D impedances produces higher voltages compared to the voltages calculated with 1-D impedances. There are also a few transmission lines that have smaller voltages across them with the use of 3-D impedances, for example, just to the west and southwest of the circled region.

5. Transmission Line Voltages for Historic Geomagnetic Storms

Each geomagnetic storm is unique. Some storms are impulsive and produce a large geomagnetic field variation over a short amount of time, while other storms are long-lived and produce relatively small magnetic field variations. The unique geomagnetic time series for each storm produces different geoelectric field variations in the solid Earth, which leads to different induced voltages across power transmission lines. The voltage across a single power line is shown for two historic geomagnetic storms (March 1989 and July 2000) in Figure 3. These storms each have different characteristics that provide an interesting comparison.

The March 1989 geomagnetic storm is most well known for causing a blackout within the Hydro-Québec power system (Bolduc, 2002), but it also caused significant anomalies within the U.S. and the mid-Atlantic regions (North American Electric Reliability Corporation, 1990). Specifically, in the mid-Atlantic region, the Elmont substation near Richmond, Virginia, experienced several issues with capacitors. The first reported issue occurred at 11:24 Coordinated Universal Time (UTC) on 13 March 1989, which corresponds to the first large rise in voltage seen in Figure 3b of Figure 3. Further issues were noted at 22:23 UTC on 13 March 1989, and 00:10 UTC on 174 March 1989, which occurred during the major portion of the storm, where calculated voltages of more than 100 V were experienced over a prolonged duration. The July 2000 geomagnetic storm exhibited large-amplitude magnetic field variations but was an impulsive event. The maximum voltage, calculated across the same transmission line, during these two storms are similar in magnitude, but the March 1989 storm produces voltages over 250 V that last for several hours. The July 2000 storm only produces voltages over 250 V for several minutes.

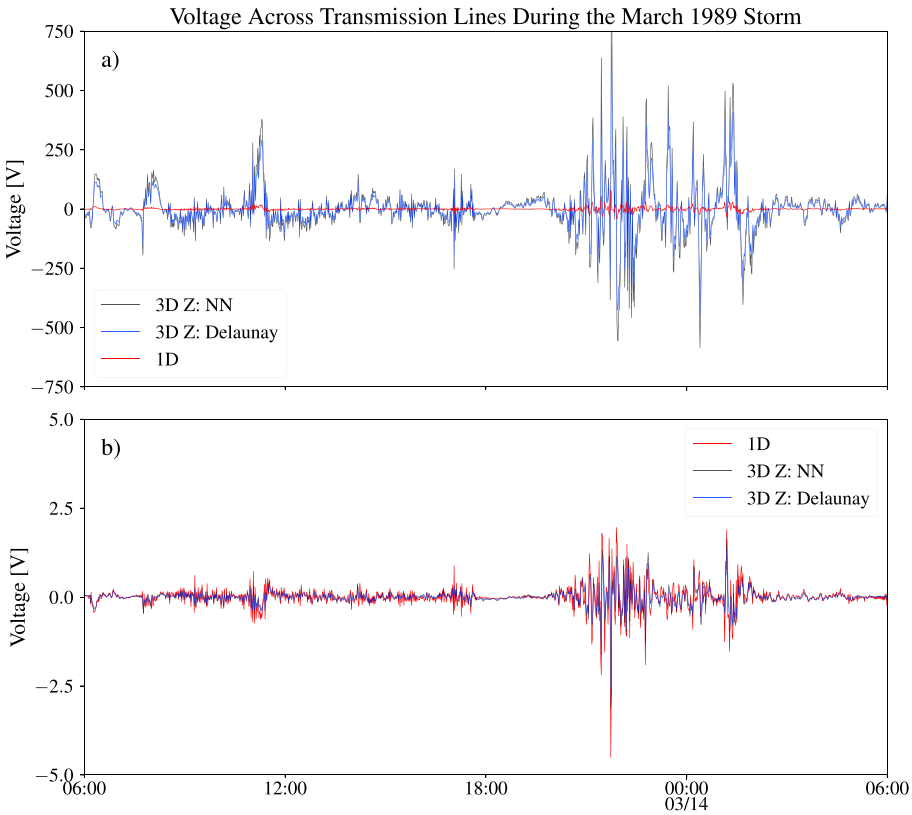

Figure 6. A time series of voltage across two transmission lines for the March 1989 geomagnetic storm. (a) A transmission line (Figure 1, Line A) where the empirical 3-D impedances produce significantly higher voltages than regional 1-D impedances (Fernberg, 2012). (b) A transmission line (Figure 1, Line B) where the empirical 3-D impe dances produce lower voltages than the regional 1-D impedances. Note the difference in scales on the *y* axis. Two different interpolation methods are presented for the calculation of empirical 3-D impedances, nearest neighbor (NN) and Delaunay, which both produce similar results. In both of the transmission lines, there are significant temporal differences in the voltage time series when using empirical 3-D impedances compared to regional 1-D impedances.

Figure 3 shows the temporal evolution of voltage for a single transmission line (Line A from Figure 1) over the duration of the two geomagnetic storms. To investigate the entire mid-Atlantic region during the geomagnetic storms, the entire transmission grid network has been animated as a movie for each storm and included in the supporting information. These animations show the calculated geoelectric field vectors and the calculated voltage within each transmission line throughout the strongest phases of each geomagnetic storm. The movies show that the areas with intense geoelectric fields correlate to the transmission lines with large voltages. It is also apparent that the direction of the geoelectric field vectors influence the transmission line voltages as well. In localized regions, if the geoelectric field vector is perpendicular to a transmission line there will be no voltage calculated across that transmission line.

Using empirical 3-D and regional 1-D impedance tensors in the mid-Atlantic region with the same geomagnetic time series and transmission grid geometry provides a direct way to analyze what influence impedance tensors have on calculated voltages across transmission lines. Figure 4 shows the electric fields calculated with the empirical EarthScope 3-D impedances and regional 1-D impedances during the March 1989 geomagnetic storm. The use of 3-D impedance tensors shows the significant geologic differences across this region with both the direction and magnitude of the electric field vectors having significant spatial variability across the region during a single snapshot in time. Using the regional 1-D impedance tensors shows slight variability in the magnitude, arising from different physiographic regions, but the directions are all the same due to the skew-symmetric nature of the 1-D impedance tensors.

The voltages across every transmission line in the mid-Atlantic are calculated with the geoelectric fields from Figure 4 and equation (3) using both NN and Delaunay interpolation. In all of the following figures the voltages calculated with Delaunay interpolation are shown. Figure 5 shows the voltages calculated across

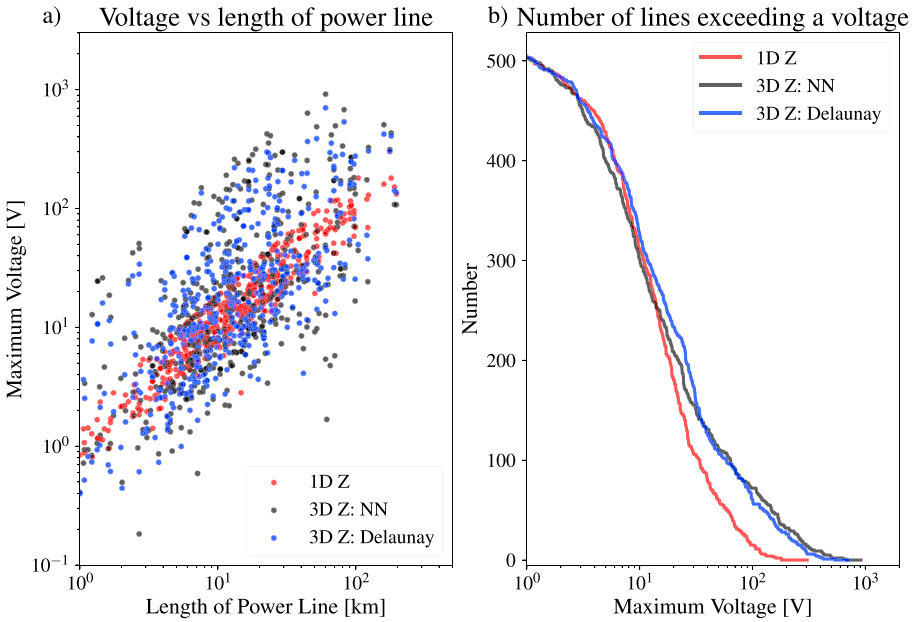

Figure 7. The maximum voltages calculated across the power lines in the Fredericksburg, VA, region during the March 1989 geomagnetic storm. (a) The maximum voltage for different lengths of lines and different interpolation methods. The use of empirical 3-D impedances leads to significantly more variability, leading some short transmission lines having large voltages across them. (b) The cumulative number of lines in the region that exceed a maximum voltage. There are more transmission lines exceeding large threshold voltages in this region when using empirical 3-D impedances relative to 1-D impedances.

the transmission lines using empirical 3-D impedances and regional 1-D impedances. The circled region is an area where the use of empirical 3-D impedances produces higher voltages compared to the voltages calculated with 1-D impedances. To the west and southwest of the circled region, several transmission lines have smaller calculated voltages when using empirical 3-D impedances.

The geoelectric field vectors in Figure 4b, obtained using empirical 3-D impedances, show substantial geographic differences in direction at this instant in time. Specifically, there are several geoelectric vectors that are pointing to the west-northwest. On the other hand, the geoelectric field vectors produced with 1-D impedances, shown in Figure 4c, all point in the same direction at any instance in time, predominantly north at this instant. Taking the angles of the geoelectric field vectors into account when integrating across a transmission line, equation (3), means that at this instant in time the east-west transmission lines will have small calculated voltages when using 1-D impedances because of the direction of the transmission lines.

The directional influence is highlighted in the circled region of Figure 5. This region has several predominantly east-west transmission lines that have large voltages when using empirical 3-D impedances, but relatively small voltages when using regional 1-D impedances. This indicates that the integration of realistic geoelectric fields across transmission lines does not get smoothed out to produce a similar voltage to those calculated with the use of regional 1-D impedances. Rather, the areas with significant geoelectric field differences also lead to significant differences in the calculated voltages across transmission lines. This is due to the unique coupling of multiple processes, which includes the geomagnetic field variability, the variations in solid Earth conductivity that lead to derived impedances, and the location of the power grid network.

The time series of calculated voltages during the March 1989 geomagnetic storm is shown in Figure 6 for two transmission lines. Transmission Line A in Figure 6a is 60 km long and is located near Richmond, Virginia, while Line B in Figure 6b is 8 km long and located closer to the coast. The locations of the two transmission lines are shown in Figure 1. Line A has voltages that are orders of magnitude higher when calculated using empirical 3-D impedances (black and blue) compared to the voltages calculated using regional 1-D impedances (red). Line B has an order of magnitude smaller voltages, and, in addition, has larger calculated voltages when using regional 1-D impedances, emphasizing the large variance in calculated voltages that is introduced in this region when using empirical 3-D impedance tensors. The voltages using 3-D impedances are calculated

using both interpolation methods, NN (black) and Delaunay (blue). There are slight differences between the methods, but the method of interpolation does not make a large difference on the resulting voltages relative to the use of empirical 3-D impedances versus regional 1-D impedances. This is likely due to the relatively close 70 km spacing of the empirical impedances. Therefore, the method of interpolation chosen does not impact the results here, but the method of interpolation could lead to a more significant difference with a coarser spacing of the impedance data.

With 1-D modeled impedances, the voltages across transmission lines follow an approximately linear trend with the length of the line because the impedances do not significantly change along one line. Figure 7a shows the maximum voltage across all of the different lengths of transmission lines in the mid-Atlantic region. The use of empirical 3-D impedances adds significant variance to the voltages across transmission lines, and it also shows that some of the highest voltages can occur in relatively short transmission lines. Figure 7b shows the cumulative number of transmission lines exceeding a given voltage. Using empirical 3-D impedances, 62 transmission lines exceed 100 V when utilizing regional 1-D impedances.

6. Discussion

The mid-Atlantic region of the United States is a very complex geologic area. The complexity of the geology leads directly to the complexity of the impedances of the solid Earth and therefore the calculated geoelectric fields within the region. Figure 4 showed a representative snapshot of the geoelectric fields during the March 1989 geomagnetic storm calculated with regional 1-D impedances and empirical 3-D impedances. The use of regional 1-D impedances misses a lot of the geologic complexity of the region. The empirical 3-D Earth impedances capture more of the underlying geologic complexity. It should also be stressed that there is likely finer geoelectric structure between the 70 km spacing of EarthScope survey stations which could be identified with a denser survey in the highly variable geoelectric regions. The continued collection of magnetotelluric data will enhance our geoelectric knowledge across the United States.

For the calculation of geomagnetically induced currents, earlier studies have suggested that the integration across transmission lines may smooth out the geoelectric variability (e.g., Viljanen et al., 2012). We have shown that the integration of the geoelectric field along power transmission lines to produce a voltage does not necessarily smooth out the variability of geoelectric fields. Rather, the calculation of voltages depends on several length scales, including the geomagnetic field variation, solid Earth conductivity throughout the region, and the location of the power grid network that leads to a complex coupling of the variables within the region. Integrating the geoelectric fields calculated with empirical 3-D impedances along the transmission lines within the region produced 62 transmission lines that exceeded 100 V compared to only 16 transmission lines exceeding 100 V when using regional 1-D impedances to calculate the geoelectric fields in the region. These results suggest that the North American Electric Reliability Corporation benchmarks (North American Electric Reliability Corporation, 2016) for geomagnetically induced currents could be revisited and updated to include a stronger emphasis on using empirical data.

In this paper, we have utilized the best available empirical data when calculating voltages across transmission lines. The methods developed here can be applied to freely available data sets across the United States to produce a better estimate of voltages, and therefore geomagnetically induced currents, within the power grid.

Acknowledgments
We thank E. Joshua Rigler, Carol A. Finn, and Jill McCarthy for reviewing a draft version of this manuscript. The magnetic field data (USGS, 1901) can be downloaded from the USGS Geomagnetism program https://geomag.usgs.gov. EarthScope impedance tensors (Schultz et al., 2006) were retrieved on 30 October 2017 from the Data Management Center of the Incorporated Research Institutions for Seismology SPUD EMTF database (Kelbert et al., 2011) https://doi.org/10.17611/DP/EMTF/USARRAY/TA. The transmission line data are obtained from the Department of Homeland Security open data website https://hifld-geoplatform.opendata.arcgis.com/. Greg Lucas' work is supported by a Mendenhall Postdoctoral Fellowship from the USGS. USArray MT TA project was led by PI Adam Schultz and Gary Egbert. They would like to thank the Oregon State University MT team and their contractors, lab and field personnel over the years for assistance with data collection, quality control, processing, and archiving. They also thank numerous districts of the U.S. Forest Service, Bureau of Land Management, the U.S. National Parks, the collected State land offices, and the many private landowners who permitted access to acquire the MT TA data. USArray TA was funded through NSF grants EAR-0323311, IRIS Subaward 478 and 489 under NSF Cooperative Agreement EAR-0350030 and EAR-0323309, IRIS Subaward 75-MT under NSF Cooperative Agreement EAR-0733069 under CFDA 47.050, and IRIS Subaward 05-OSU-SAGE under NSF Cooperative Agreement EAR-1261681 under CFDA 47.050.

References

Bedrosian, P. A., & Love, J. J. (2015). Mapping geoelectric fields during magnetic storms: Synthetic analysis of empirical United States impedances. *Geophysical Research Letters*, *42*, 10,160–10,170. https://doi.org/10.1002/2015GL066636

Bolduc, L. (2002). GIC observations and studies in the Hydro-Québec power system. *Journal of Atmospheric and Solar-Terrestrial Physics*, *64*(16), 1793–1802. https://doi.org/10.1016/S1364-6826(02)00128-1

Bonner, L. R., & Schultz, A. (2017). Rapid prediction of electric fields associated with geomagnetically induced currents in the presence of three-dimensional ground structure: Projection of remote magnetic observatory data through magnetotelluric impedance tensors. *Space Weather*, *15*, 204–227. https://doi.org/10.1002/2016SW001535

Boteler, D. (2014). Methodology for simulation of geomagnetically induced currents in power systems. *Journal of Space Weather and Space Climate*, *4*(A21), 11. https://doi.org/10.1051/swsc/2014018

Boteler, D. H. (2001). Space weather effects on power systems. In D. H. Boteler (Ed.), *Space Weather* (pp. 347–352). Washington, DC: American Geophysical Union.

Boteler, D. H., & Pirjola, R. J. (2017). Modeling geomagnetically induced currents. *Space Weather*, *15*, 258–276. https://doi.org/10.1002/2016SW001499

Egbert, G. D. (2007). Robust electromagnetic transfer functions estimates. In G. D. Egbert (Ed.), *Encyclopedia of geomagnetism and paleomagnetism* (pp. 866–870). Netherlands: Springer.

Electric Power Research Institute (2013). How to calculate electric fields to determine geomagnetically-induced currents.

Federal Energy Regulatory Commission (2013). *Reliability standards for geomagnetic disturbances* (Vol. 78). Federal Register, Rules and Regulations.
Fernberg, P. (2012). One-dimensional Earth resistivity models for selected areas of continental United States and Alaska. *EPRI Technical Update*, *1026430*, 1–190.
Kelbert, A., Balch, C. C., Pulkkinen, A., Egbert, G. D., Love, J. J., Rigler, E. J., & Fujii, I. (2017). Methodology for time-domain estimation of storm time geoelectric fields using the 3-D magnetotelluric response tensors. *Space Weather*, *15*, 874–894. https://doi.org/10.1002/2017SW001594
Kelbert, A., Egbert, G. D., & Schultz, A. (2011). IRIS DMC data services products: EMTF. The magnetotelluric transfer functions. https://doi.org/10.17611/DP/EMTF.1
Love, J. J., & Finn, C. A. (2011). The USGS geomagnetism program and its role in space weather monitoring. *Space Weather*, *9*, S07001. https://doi.org/10.1029/2011SW000684
Love, J. J., Lucas, G. M., Kelbert, A., & Bedrosian, P. A. (2017). Geoelectric hazard maps for the Mid-Atlantic United States: 100-year extreme values and the 1989 magnetic storm. *Geophysical Research Letters*, *45*, 5–14. https://doi.org/10.1002/2017GL076042
Love, J. J., Pulkkinen, A., Bedrosian, P. A., Jonas, S., Kelbert, A., Rigler, E. J., … Black, C. E. (2016). Geoelectric hazard maps for the continental United States. *Geophysical Research Letters*, *43*, 9415–9424. https://doi.org/10.1002/2016GL070469
Marti, L., Rezaei-Zare, A., & Yan, A. (2013). Modelling considerations for the Hydro One real-time GMD management system. In *2013 IEEE Power Energy Society General Meeting* (pp. 1–6). https://doi.org/10.1109/PESMG.2013.6673069
Marti, L., Yiu, C., Rezaei-Zare, A., & Boteler, D. (2014). Simulation of geomagnetically induced currents with piecewise layered-Earth models. *IEEE Transactions on Power Delivery*, *29*(4), 1886–1893. https://doi.org/10.1109/TPWRD.2014.2317851
Molinski, T. S. (2002). Why utilities respect geomagnetically induced currents. *Journal of Atmospheric and Solar-Terrestrial Physics*, *64*(16), 1765–1778. https://doi.org/10.1016/S1364-6826(02)00126-8
National Research Council (2008). Severe space weather events: Understanding societal and economic impacts: A workshop report.
North American Electric Reliability Corporation (1990). March 13, 1989 geomagnetic disturbance, The 1989 system disturbances.
North American Electric Reliability Corporation (2013a). Application guide: Computing geomagnetically-induced current in the bulk-power system.
North American Electric Reliability Corporation (2013b). Geomagnetic disturbance planning guide.
North American Electric Reliability Corporation (2016). Benchmark geomagnetic disturbance event description, Project 2013-03 GMD mitigation.
Overbye, T. J., Shetye, K. S., Hutchins, T. R., Qiu, Q., & Weber, J. D. (2013). Power grid sensitivity analysis of geomagnetically induced currents. *IEEE Transactions on Power Systems*, *28*(4), 4821–4828. https://doi.org/10.1109/TPWRS.2013.2274624
Piccinelli, R., & Krausmann, E. (2014). Space weather and power grids vulnerability assessment, Publications office of the European Union, Institute for the Protection and Security of the Citizen.
Preparata, F. P., & Shamos, M. I. (1993). *Computational geometry: An introduction*. New York: Springer.
Price, P. R. (2002). Geomagnetically induced current effects on transformers. *IEEE Transactions on Power Delivery*, *17*(4), 1002–1008. https://doi.org/10.1109/TPWRD.2002.803710
Samuelsson, O. (2013). *Geomagnetic disturbances and their impact on power systems* (pp. 1–18). Lund, Sweden: Industrial Electrical Engineering and Automation, Lund University.
Schultz, A. (2010). EMScope: A continental scale magnetotelluric observatory and data discovery resource. *Data Science Journal*, *8*, IGY6–IGY20.
Schultz, A., Egbert, G. D., Kelbert, A., Peery, T., Clote, V., Fry, B., … National geoelectromagnetic facility (2006). USArray TA magnetotelluric transfer functions. https://doi.org/10.17611/DP/EMTF/USARRAY/TA
Shetye, K., & Overbye, T. (2015). Modeling and analysis of GMD effects on power systems: An overview of the impact on large-scale power systems. *IEEE Electrification Magazine*, *3*(4), 13–21. https://doi.org/10.1109/MELE.2015.2480356
Simpson, F., & Bahr, K. (2005). *Practical magnetotellurics*. Cambridge, UK: Cambridge University Press.
USGS (1901). USGS geomagnetism program definitive data, INTERMAGNET, Other/Seismic Network. Retrieved from https://doi.org/10.7914/SN/NT
Viljanen, A., Pirjola, R., Wik, M., Ádám, A., Prácser, E., Sakharov, Y., & Katkalov, J. (2012). Continental scale modelling of geomagnetically induced currents. *Journal of Space Weather and Space Climate*, *2*, A17. https://doi.org/10.1051/swsc/2012017
Watermann, J., Rasmussen, O., Stauning, P., & Gleisner, H. (2006). Temporal versus spatial geomagnetic variations along the west coast of Greenland. *Advances in Space Research*, *37*(6), 1163–1168. https://doi.org/10.1016/j.asr.2005.08.019
Weigel, R. S. (2017). A comparison of methods for estimating the geoelectric field. *Space Weather*, *15*, 430–440. https://doi.org/10.1002/2016SW001504